Targeted rescue of synaptic plasticity improves cognitive decline in sepsis-associated encephalopathy

Benedikt Grünewald[1,2,4], Jonathan Wickel[1,2], Nina Hahn[1,2], Franziska Hörhold[1,3], Hanna Rupp[1,2], Ha-Yeun Chung[1,2], Holger Haselmann[1,2], Anja S. Strauss[2], Lars Schmidl[2], Nina Hempel[2], Lena Grünewald[5], Anja Urbach[2], Markus Blaess[1,6], Ralf A. Claus[1,3], Rainer König[1,3], Christian Geis[1,2,*]

[1]Center for Sepsis Control and Care, [2] Section Translational Neuroimmunology, Department of Neurology, [3]Department of Anesthesiology and Intensive Care, Jena University Hospital, Am Klinikum 1, 07747 Jena, Germany; [4] Institute of Pathophysiology, University Medical Center of the Johannes Gutenberg University Mainz, 55131 Mainz, Germany, [5] Department of Psychiatry, Psychosomatic Medicine and Psychotherapy, University Hospital of Frankfurt, 60528 Frankfurt, Germany, [6] Institute of Precision Medicine, Medical and Life Sciences Faculty, Furtwangen University, 78054 Villingen-Schwenningen, Germany

*lead contact

Corresponding author:

Christian Geis, MD

Section Translational Neuroimmunology

Department of Neurology, Am Klinikum 1, 07747 Jena, Germany

email: christian.geis@med.uni-jena.de

phone: +49-3641-9323410

fax: +49-3641-9323422

Running title: Synaptic rescue of post-sepsis memory defects

Abstract

Sepsis-associated encephalopathy (SAE) is a severe and frequent complication in patients with systemic infection resulting in delirium, premature death, and long-term cognitive impairment. The underlying pathophysiology of SAE is largely unresolved and treatment options are missing. We report that experimental sepsis in mice induces synaptic pathology in the brain underlying defective long-term potentiation and cognitive dysfunction. Genes related to neuronal and synaptic signaling in the brain, e.g. the activity-regulated cytoskeleton-associated protein (*Arc/Arg3.1*), the transcription-regulatory EGR family, and the dual-specificity phosphatase 6 (*Dusp6*) were downregulated. On the protein level, ARC expression and mitogen-activated protein (MAP) kinase signaling in the brain were affected during SAE. For targeted rescue of dysregulated synaptic signaling and plasticity we overexpressed ARC in the hippocampus by microinjection of an adeno-associated virus containing a neuron-specific plasmid of the ARC transgene. Defective synaptic plasticity in the hippocampus was restored and memory improved. Moreover, synaptic plasticity, neuronal spine pathology, and memory dysfunction also improved when post-septic mice were subjected to enriched environment demonstrating the potential for activity-induced recovery. Together, we identified synaptic pathology of neurocognitive dysfunction after severe systemic infection and provide a proof-of-concept approach to interfere with SAE pathomechanisms leading to cognitive improvement.

Introduction

Sepsis is a world-wide health problem with increasing incidence and high mortality. Current guidelines define sepsis as life-threatening organ dysfunction caused by a dysregulated host response to infection (Singer et al., 2016). Recent epidemiological studies revealed an incidence rate of 437 hospital-treated sepsis patients per 100.000 person-years and a global incidence of 31.5 million sepsis cases with 5.3 million deaths annually (Fleischmann et al., 2016). Sepsis-associated encephalopathy (SAE) is a frequent complication, often presents as the initial symptom, and was also shown to be an independent risk factor for increased

mortality (Ely et al., 2004). Depending on definition, the frequency of SAE occurs in up to 70% of patients with severe sepsis, however prospective studies providing an accurate estimate of SAE incidence are missing (Eidelman et al., 1996; Gofton and Young, 2012). Moreover, long-term neuropsychiatric defects are now increasingly recognized also in patients after severe systemic infection, e.g. by SARS-CoV2. Among diverse neuropsychiatric sequelae following COVID-19, cognitive dysfunction is considered as serious manifestation, thus adding to a contemporary medical problem with so far unpredictable dimension (Taquet et al., 2021).

The early phase of SAE during the infectious period manifests with delirium-associated symptoms such as agitation, psychotic experiences, and sleep disturbances. In the later phase patients typically suffer from long-term cognitive deficits comparable to those found in patients with beginning Alzheimer´s dementia (Chung et al., 2020; Pandharipande et al., 2013). The etiology of SAE is likely multifactorial including blood-brain barrier dysfunction, ischemia and hemorrhages, changes in cerebral homeostasis, and dysregulation of cholinergic neurotransmission (Chung et al., 2020; Gofton and Young, 2012; Mazeraud et al., 2020). It is conceivable that severe systemic inflammation leads to activation of cerebral immune cells, e.g. microglia thereby inducing a pathological proinflammatory milieu in the brain (Mazeraud et al., 2020; Michels et al., 2020; Semmler et al., 2008; Shemer et al., 2020; Trzeciak et al., 2019; Widmann and Heneka, 2014; Zrzavy et al., 2019). However, the pathophysiology of SAE is only incompletely understood and causal therapeutic options are missing. Specifically, it is unclear how sepsis-induced neuroinflammation mediates persistent neuronal and synaptic dysfunction finally leading to neurocognitive defects.

Using a large-scale and multidisciplinary approach, we here present the synaptic pathophysiology of SAE in a mouse model of peritoneal polymicrobial sepsis. By identifying severely impaired pathways of synaptic plasticity, we were able to establish therapeutic interventions leading to rescue of neuronal functionality finally resulting in improvement of

disease symptoms. Specifically, targeting defective regulatory mechanisms of synaptic plasticity offers conceptual advances for translational strategies in SAE.

Results and Discussion

We induced severe experimental sepsis in male 769 C57BL/6J mice by polymicrobial peritonitis after intraperitoneal injection of a standardized and microbiologically validated human faeces material (peritoneal contamination and infection model, PCI) (Gonnert et al., 2011) (Fig. 1 A). Mice showed a median disease severity of 12.25 on the 5 day PCI Clinical Severity Score (CSS) (Fig. 1 B) and only surviving mice with a 5 day CSS ≥ 11.5, indicating severe sepsis, were included for further experiments (n = 309 PCI). Concomitant antibiotic rescue therapy with meropenem (weeks 1 and 2) and enrofloxacin from week 3 led to a survival rate of 0.38 after 8 weeks (Fig. 1 B). In the late stage 8 weeks after PCI induction, surviving mice displayed delayed learning and defective memory performance as revealed by Morris water maze (MWM) test. Deficits started from day 1 of the learning phase and memory dysfunction persisted also in the recall phase on day 8 (Fig. 1C). Moreover, mice had increased anxiety-like behavior in elevated plus maze test (EPM, Fig. 1D) and in the open field (OF, Fig. 1E). These findings can be specifically attributed to sepsis-induced brain dysfunction and were not caused by post-sepsis related sickness, as the overall phenotype was normal with recovered body weight and regular locomotor activity (Fig. 1 D and E). In order to identify the underlying pathophysiology of cognitive dysfunction we tested synaptic plasticity by recording local field potentials in the CA1 region of the hippocampus after stimulation of Schaffer collaterals. We found severely affected long-term potentiation (LTP) at late time points after PCI (Fig. 1F). Together, these data demonstrate that severe systemic infection results in long-term neurocognitive deficits. Persistent cognitive decline in the late phase after surviving sepsis is substantiated by defective hippocampal LTP.

Next, we investigated synaptic transmission in the hippocampus post-sepsis by whole-cell patch-clamp recordings in dentate gyrus granule cells. We found reduced frequency of

quantal excitatory postsynaptic currents (miniature, mEPSCs, Fig. 1G) and spontaneous EPSCs (sEPSCs, Fig. 1H) which is indicative for overall reduction of excitatory presynaptic terminals. Unexpectedly, peak amplitudes of mEPSCs, of sEPSCs, and of minimally evoked EPSCs (eEPSCs, Fig. 1I) after stimulation of the medial perforant pathway were increased (Fig. 1 G to I) whereas EPSC kinetics were unchanged (rise and decay time, data not shown) which might reflect increased recruitment of AMPA receptors to postsynaptic sites, e.g. in a homeostatic scaling mechanism.

In order to obtain mechanistic insight in the molecular pathomechanism of sepsis-induced neuronal dysfunction, we next investigated the transcriptional profile of brain tissue of acute septic mice (day 3 after PCI), of mice at a late stage after surviving sepsis (week 10), and of respective controls. We found differently regulated brain gene expression early after sepsis, whereas after 10 weeks gene expression was rather similar to controls (Fig. S1). Gene Ontology (GO) term enrichment analysis of differentially expressed genes (DEGs) at day 3 revealed that transcripts related to neuronal function (e.g., GO terms ‘synapse’, ‘postsynaptic density’, ‘dendrite’) are severely downregulated (Fig. 2). As expected, transcripts related to inflammation (e.g. GO terms ‘innate immune response’, ‘inflammatory response’) and to gene transcription were upregulated. Against this, in the late stage after sepsis, inflammatory pathways in the brain were no longer disturbed and pathways related to gene transcription were downregulated. Moreover, genes associated to neuronal function (e.g. GO terms ‘neuron projection’, ‘dendrite’) were upregulated, most likely in a compensatory way. The most prominently downregulated gene was *Arc*, encoding activity-regulated cytoskeleton-associated protein ARC/ARG3.1 (ARC), a master regulator of synaptic plasticity (Shepherd and Bear, 2011) (Fig. 3A and B). Protein interaction network of corresponding DEGs on day 3 after PCI revealed downregulation of genes encoding close ARC interaction partners, thus predicting a major role in dysfunctional synaptic plasticity and signaling (Fig. 3A). Genes of the early growth response protein (*Egr*) family, transcription regulatory factors involved in neuronal plasticity (Li et al., 2005), as well as *Dusp6*, encoding the ERK-directed dual-specificity phosphatase 6, *Nrgn*, encoding Neurogranin/RC3, a calmodulin-binding protein

involved in CaMKII dependent synaptic plasticity (Pak et al., 2000), and *Mapk11*, encoding p38 Mitogen-activated protein kinase 11, were downregulated (Fig. 3 A and B). On the protein level, we indeed found reduction of ARC and of activated ERK, an upstream mitogen-activated protein (MAP) kinase relevant in transcription of immediate-early genes such as *Arc* (Huang et al., 2007) after PCI (Fig. 3 C and D; Fig. S2). Together, these data indicate that severe neuroinflammation parallels alteration of synaptic regulatory pathways in early stages together with reactive gene regulation patterns. Impaired neuronal functionality itself converges on activity-regulated pathways important for synaptic plasticity. Based on these findings, we then followed two interventional strategies to rescue defective synaptic plasticity and cognitive dysfunction after PCI. First, we specifically targeted the PCI-induced downregulation of the synaptic master regulator ARC. Second, in a more general concept, we subjected mice to enriched environment (EE) which is known to have beneficial effects for cognitive performance by enhancing synaptic plasticity, e.g. due to activation of activity-regulated genes (van Praag et al., 2000).

ARC is abundantly expressed in somata and dendrites of CamKII positive excitatory neurons in the CNS (Vazdarjanova et al., 2006). It is an important, bidirectional regulator of long-term synaptic plasticity including LTP, long-term depression (LTD), heterosynaptic LTD, and homeostatic synaptic scaling (Shepherd and Bear, 2011). ARC mediates activity-regulated trapping of AMPA receptors at postsynaptic sites by interaction with the endocytic machinery and PSD-95 complexes (Zhang et al., 2015). In *Arc* knockout (ko) mice and after *Arc* silencing using antisense oligonucleotides, LTP consolidation and memory formation is impaired (Guzowski et al., 2006; Plath et al., 2006). Furthermore, ARC regulates synaptic AMPA receptor expression dependent on synaptic activity representing the key mechanism of homeostatic plasticity (Korb et al., 2013; Okuno et al., 2012). Persistent deficiency of ARC leads to upscaling of AMPA receptor expression (Shepherd et al., 2006) which is consistent with increased AMPA receptor mediated EPSC peak amplitude in synaptic transmission observed here in mice after PCI (Fig. 1 G to I). To overcome the manifest and not activity-dependent PCI-induced synaptic downregulation of ARC, we constitutively overexpressed

ARC in the hippocampus of post-septic mice using an adeno-associated virus containing a neuron-specific bicistronic plasmid of the *Arc* and *Venus* transgene under the synapsin promotor (*Arc*-AAV; Fig. 4A). Bilateral *in-vivo* injection of *Arc*-AAV in three injection sites of the hippocampus led to robust, constitutively driven and not activity-dependent upregulation of ARC in hippocampal neurons (Fig. 4B). According to previous studies showing inverse regulation of synaptic AMPA receptor expression by synaptic scaling mechanisms after *Arc* overexpression (DaSilva et al., 2016; Jenks et al., 2017; Rial Verde et al., 2006) we expected affected LTP due to disturbed AMPA receptor mediated signaling in non-septic control mice after *Arc* overexpression. Indeed, we found reduced LTP in the Schaffer collateral-CA1 pathway in patch-clamp single cell recordings of non-septic control mice after *Arc*-AAV injection (Fig. S3A to C).

PCI surviving mice that received injection of the empty control vector expressing only fluorescent Venus showed again learning and memory dysfunction also in the Barnes maze (BM) 8 weeks after PCI, similar to the PCI induced alterations in the MWM (Fig. 4C). Importantly, hippocampal *Arc* overexpression in PCI mice induced improvement of spatial learning and memory recall (Fig. 4C). As expected, *Arc* overexpression in SHAM mice did not improve cognitive function (Fig. S3D). Locomotor function was not affected in all experimental groups (Fig. S3E and F). Fear-related behavior as measured in the EPM was present in PCI mice and did not improve upon *Arc* overexpression in the hippocampus since it is primarily mediated by signaling pathways in the amygdala (Fig. S3F). Corroborating the behavioral findings, hippocampal LTP of PCI mice after *Arc*-AAV injection was rescued to almost normal values when compared to sham mice with injection of *control*-AAV (Fig. 4D). These data indicate that increasing ARC protein levels in the hippocampus is sufficient to at least partially reverse sepsis-induced neuronal dysfunction and defective synaptic plasticity mechanisms, which are responsible for persistent cognitive impairment.

These data led us to hypothesize that not only constitutive upregulation of a key regulating synaptic plasticity protein, but also stimulus-induced activation, in general, can improve

cognitive dysfunction in mice after experimental sepsis. We therefore tested if an established EE paradigm (van Praag et al., 2000) is also capable of rescuing defective synaptic plasticity and memory dysfunction after PCI (Fig. 5A). Among a variety of mechanisms, EE can enhance adult neurogenesis and induce synaptic plasticity pathways by increasing BDNF and trkB signaling and by activation of activity-regulated genes such as ARC (Ramirez-Amaya et al., 2005). First, we again reproduced PCI-induced long-term cognitive dysfunction in the BM 8 weeks after PCI, anxiety-related behavior in the EPM, and defective LTP in mice without special housing conditions (PCI versus SHAM non-enriched (NE); Fig. 5B to D). To substantiate these functional defects, we additionally quantified synaptic spines in apical dendrites of hippocampal CA1 neurons providing morphological information on plasticity changes. The overall spine density and, more specifically, mature mushroom spines were reduced corroborating the findings of defective LTP and may reflect defective ARC interaction with actin-binding proteins (Fig. 5E). Importantly, when PCI mice were subjected to 6 weeks of EE housing conditions, they showed improved performance in the BM test 8 weeks after PCI and reduced anxiety-related behavior in the EPM (Fig. 5B and C). Again, possible confounders as sickness behavior and locomotor hypoactivity were not present in any of the experimental groups at 8 weeks after PCI (Fig. S3G). Synaptic plasticity as measured by hippocampal LTP was preserved and reduction of synaptic spines was no longer present in PCI mice after EE (Fig. 5 D and E).

Together, our findings identify defective regulation of synaptic plasticity as a key pathogenic mechanism of long-term cognitive dysfunction in SAE. Specifically, synaptic expression of ARC and upstream signaling interaction partners are affected. Targeting these pathways offers conceptual advances for translational strategies in SAE. Future therapeutic strategies may therefore comprise general activation, e.g. by personalized cognitive training approaches that need evaluation in controlled clinical trials. The current findings further encourage patient-oriented activation training beginning at early stages in the disease course. Moreover, the identification of impaired neuronal pathways in SAE provides first opportunity for targeted intervention strategies. Increasing ARC levels, e.g. by stimulation of

upstream pathways such as neurotrophin BDNF receptor/TrkB activation, ERK signaling, or CREB phosphorylation (Jenks et al., 2017; Nagahara et al., 2009; Panja and Bramham, 2014; Yin et al., 2002), may be promising starting points for target-directed therapies. On a broader scale and with respect to the rapidly increasing amount of patients suffering from cognitive dysfunction after SARS-CoV-2 infection in the current pandemic, it will be important to see if here identified pathways can also attribute to neurocognitive dysfunction in post-COVID syndrome and other systemic infectious disease.

Methods

Peritoneal contamination and infection (PCI) mouse model of experimental sepsis

All animal experiments were approved by the state authorities of Thuringia (UKJ-02-085-14) and were performed in accordance with animal welfare and the ARRIVE guidelines (Kilkenny et al., 2010). All efforts were made to minimize animal suffering and to reduce the number of animals used. Experimental sepsis was induced by the standardized and established PCI model as described previously (Gonnert et al., 2011). In brief, PCI mice received an intraperitoneal injection of human fecal slurry (diluted 1:4 in saline solution, 3 µl/g B.W.) with a 21-gauge cannula. Control mice were injected with 100µl of 0.9 M saline solution. We exclusively used male C57Bl6J mice as PCI disease severity may vary in female mice due to the menstrual cycle and hormonal fluctuations. Mice were closely monitored and the Clinical Severity Score (CSS, grade 1 to 4) was assessed as described previously (Gonnert et al., 2011): grade 1: No signs of illness, active and curious, quick movements upon exogenous stimuli, normal posture; grade 2: Low-grade illness, less active with occasional interruptions in activity, reduced alertness, but adequate response to exogenous stimuli, posture slightly hunched; grade 3: Mid-grade illness, slow and sleepy, moves with difficulty, limited and delayed reaction to exogenous stimuli, hunched posture; High-grade illness, mouse lethargic, motionless, no spontaneous movement, no reaction to exogenous stimuli, severely hunched

posture. To avoid premature death due to acute severe peritonitis, mice were systemically treated with antibiotics. PCI mice received the first subcutaneous (s.c.) injection of the beta-lactam antibiotic meropenem (650µl, 1mg/ml) when the CSS reached a point value of 3. To increase long-time survival after PCI, meropenem was s.c. injected b.i.d. for 7 days and one time per day at the following three days. Thereafter, enrofloxacin (Baytril 2,5%, Bayer AG, Germany) was added to the sugared drinking water (saccharose solution 2,5%) in a final concentration of 2 mg/ml until the end of the experiment. Both, PCI and control animals received equal amounts of antibiotic treatment For the experimental sepsis groups, only PCI animals with severe sepsis (cumulative 5d-CSS of ≥ 11.5) were included in further experiments.

Stereotactic intrahippocampal microinjection

Stereotactic surgery for injection of AAV into the hippocampus were performed as previously described (Haselmann et al., 2015). Briefly, mice were deeply anesthetized by 1.5 to 2.0% of isoflurane/oxygen and head fixed into a stereotactic apparatus (Lab StandardTM, Stoelting, Wood Dale, IL, USA). The skull was exposed by a midline incision, stereotactic injection sites were marked, and holes were drilled with a dentist driller (Foredom, Bethel, CT, USA). Injections of AAV were performed at three sites within the hippocampus: coordinates in mm with respect to bregma (AP/L/DV): 1st (2.8/2.8/2.8); 2nd (2.1/1.4/1.4); 3rd (2.1/1.4/2.1). Very thin injection pipettes were pulled from borosilicate glass (WPI, Sarasota, FL,USA, #4878) and filled with AAV preparation (concentration 1x10^10gc/µl) in 0.9 M saline solution. The injection pipette was placed at stereotactic coordinates and 1 µl of AAV containing solution was injected with an injection speed of 0.4 nl/s by a microprocessor controlled nanoliter injector (Nanoliter 2000 + SYS-Micro4 Controller, WPI) per injection site. Tissue damage in the target region was avoided by use of very thin glass application pipettes, low injection volume, and slow injection speed. After injections the skin of the animals was sutured and mice were taken back to their home cage.

Behavioral analysis

Behavioral analyses were performed at 8 weeks after PCI to assure long-term behavioral dysfunction after experimental sepsis.

Open Field (OF)

OF testing was performed similar to a previously described protocol (Grünewald et al., 2017). Here, a custom-made square-shaped box (50x50 cm) was used with walls impermeable for light. The box was open to allow filming and illumination. The arena was divided into a center zone (25x25 cm) and the surrounding periphery zone. Due to shadows arising from the walls of the OF, illumination at the floor level slightly decreased from the center (180-200 lux) to the periphery (120-150 lux). Individual animals were placed in the arena adjacent and oriented towards the wall. Mice were allowed to explore the OF for 5 minutes while the animals were videotaped and tracked (EthoVision, Noldus, Wageningen, Netherlands, or ANYmaze, Stoelting Europe, Dublin, Ireland). Parameters measured included total time spent in center zone or periphery zone, total distance travelled, and number of entries into the zones. After completion of a trial, OF was cleaned with 70% ethanol to ensure identical experimental conditions for the subsequent trial.

Elevated Plus Maze (EPM)

A custom-made EPM consisting of grey plastic was used. The EPM was elevated 100 cm above the floor level and had two opposing open and two closed arms (31 x 5,8 cm) as well as an intersection (5,8 x 5,8 cm). The closed and open arms, and the intersection were illuminated with 40, 160 and 120 Lux, respectively. Mice were placed in the intersection facing to an open arm and locomotion was tracked for 5 minutes. The number of arm entries and the time spent in closed and open arms as well as the intersection were recorded using a camera tracking system (EthoVision or ANYmaze). An arm entry was defined by all four

feet being set in the respective arm. The EPM was cleaned using 70% ethanol after each trail to ensure equal experimental conditions.

Morris Water Maze (MWM)

A custom-made MWM of 119 cm diameter was used which was covered with white foil and illuminated with 30 Lux. The water temperature was set to 20 °C and water was supplemented with milk for better tracking of C57Bl/6J mice and to prevent that mice can visually identify the hidden platform. The diameter of the platform was 10.5 cm and it was placed 1.5 cm below the water surface. Four quadrants were subdivided by clearly distinguishable landmarks placed around the MWM. On day -1 mice were placed in the MWM for 60 s without hidden platform for habituation. Thereafter, mice were subjected to testing in the MWM for 7 consecutive days with 3 trials per day. Here, mice were placed in the water facing towards another quadrant in every trial in a predetermined manner. Time and the distance moved until mice reached the platform were determined. Mice had to enter the platform and had to stay on the platform for 3 s for evaluation of the trial being successful. Trial was terminated by the investigator when mice did not find the platform within 60 s and mice where then gently moved to the platform to assure learning in every trial. On the following day (day 8) a probe trial was conducted. Here, the hidden platform was removed and the time spent and distance travelled in the target quadrant (previous position of the platform) was determined. Tracking was performed using ANYmaze.

Barnes Maze (BM)

A circular white PVC platform (diameter 120 cm), mounted on a rotatable stand, elevated 100 cm above floor level, and consistently illuminated by 2 light sources (900-1000 Lux) was used. Three different cues (black-colored geometric shapes printed on paper) were placed at three walls surrounding the maze. At the open side of the maze the examiner was regarded as the cue. The maze comprised 40 pseudo-randomly distributed and equally sized holes (diameter each 5 cm). During the habituation (d0) and training phase (d1-6) 3 an escape box was mounted below one of the holes, while the other holes were closed with plastic disks

made of the same material (black PVC). 4 different holes at the respective sides of the maze were used as escape holes. The location of the escape box was kept constant for each mouse but varied between mice (total of 4 possible target locations). Before starting each experiment, mice were acclimated to the testing room for at least 30 minutes and each mouse was placed in an individual holding cage after the experiment. After each trial the maze was cleaned with 70% ethanol to ensure comparable experimental conditions. In the habituation phase (d0), mice were placed in a transparent plastic located in the center of the maze. After 60 seconds the cylinder was lifted and mice were allowed to explore the maze for 60 seconds and then gently led to the escape box using the transparent cylinder. Mice were allowed to spend 2 minutes in the escape box before they were placed in individual holding cages. Each mouse underwent the habituation phase thrice with an inter-trial interval of approximately 10 minutes. In the training phase (d1-6), an opaque instead of the transparent plastic cylinder was used. The cylinder was lifted after 20 seconds and mice were videotaped and tracked (EthoVision) for 4 minutes or until the mouse entered the escape box. In the testing phase (d7) all holes were closed. After 20 seconds in the opaque cylinder, mice were videotaped for 60 sec and the time spent and distance travelled in the target quadrant (previous position of the escape box) was determined.

Enriched environment

From day 10 after PCI, mice were housed in an enriched environment cage (6 animals/cage, 85 cm × 75 cm × 40 cm) with stimuli comprising objects (e.g. ladders and tunnels, running wheel, nesting material, and climbing boards). The configuration of the objects was changed on a weekly basis (Jankowsky et al., 2005). The control group remained in the normal standard housing conditions all over the experiment without additional stimulation of motor activity (2 animals/cage; 54 cm × 38 cm × 19 cm).

Electrophysiology

Preparation of acute hippocampal slices

Acute coronal hippocampal slices for field potential (fEPSP) recordings were prepared from adult mice. Isofluran anesthetized mice were sacrificed by decapitation and brains were dissected and sliced (400µm) using a Leica VT 1200 microtome in ice-cold high-sucrose solution (in mM): 20 NaCl, 25 $NaHCO_3$, 10 Glucose, 150 Sucrose, 4 KCl, 1.25 NaH_2PO_4, 0.5 $CaCl_2$, 7 $MgCl_2$. Slices were stored at 32°C for 30 min and subsequently at room temperature in artificial cerebrospinal fluid 1 (aCFS 1; in mM): 124 NaCl, 26 $NaHCO_3$, 10 glucose, 3.4 KCl, 1.2 NaH_2PO_4, 2 $CaCl_2$, 2 $MgSO_4$ before transferring into the recording chamber.

For whole-cell patch-clamp recordings previously published protocols were adapted (Peca et al., 2011; Zhao et al., 2011). Mice were deeply anesthetized with isoflurane and then transcardially perfused with ice-cold protective aCSF2 (in mM): 95 *N*-methyl-D-glucamine, 30 $NaHCO_3$, 20 HEPES, 25 Glucose, 2.5 KCl, 1.25 NaH_2PO4, 2 Thiourea , 5 Na-Ascorbat, 10 $MgSO_4$, 0.5 $CaCl_2$ and 12 *N*-Acetyl-L-cysteine. Brains were sliced according to previous protocols ('magic cut') (Bischofberger et al., 2006) and the slices were subsequently stored for 12 minutes in the same solution at 34°C. Afterwards slices were transferred to aCSF3 (in mM): 125 NaCl, 25 $NaHCO_3$, 25 Glucose, 2.5 KCl, 1.25 NaH_2PO_4, 2 $CaCl_2$, 1 $MgCl_2$ supplemented with (in mM) 2 Thiourea, 5 Na-Ascorbate, 3 Na-Pyruvate and 12 *N*-Acetyl-L-cysteine. All solutions were continuously purged with carbogen (95% O_2, 5% CO_2) and the pH was maintained at 7.3.

Whole-cell patch clamp analysis of the dentate gyrus

Whole cell patch clamp recordings were performed using a EPC10 amplifier (HEKA, Germany) as described previously (Grünewald et al., 2017). During the experiment slices were superfused with aCSF3 at RT. Dentate granule cell were visually identified and patched using glass pipettes (3 – 4 MΩ) filled with intracellular solution (in mM) 115 potassium gluconate, 40 KCl, 10 Hepes, 0.1 EGTA, 2 Na_2ATP, 2 $MgCl_2$. EPSC were recorded in the presence of bicucillin and CGP 52432. For the measurement of miniature EPSC TTX (1 µM) was added. Minimal stimulation at 0.3 Hz applied via an aCSF 3-filled glass pipette within the medial perforant path was used to evoke eEPSC. Stimulation of minimal evoked eEPSC was

determined by a synaptic failure rate of 50 % as reported previously (Petit-Pedrol et al., 2018).

Analysis of long-term potentiation (LTP) by recordings of fEPSP

Measurements of fEPSP at the Schaffer collateral (SC) - CA1 synapses were performed as described (Planaguma et al., 2016). Slices were perfused with aCSF1 at 2.5 ml/min at 32-33°C. Stimulation within SC was performed using a stimulation isolation unit (Isoflex A.M.P.I, Jerusalem, Israel) and costume made bipolar platinum electrodes. Glass electrodes filled with aCSF1 in the stratum radiatum were used to record the fEPSP. Stimulation strength was varied between 25 and 400µA to record the input-output curve. For subsequent recordings the stimulation strength was adjusted by reducing the stimulation by 10% from the lowest strength which evoked a fEPSP with a discernable population spike. Stimuli were delivered at 0.03 Hz. LTP was induced after a baseline recording of 15 min by 20 theta bursts of 4 pulses of 100 Hz with an interval of 200 ms. After induction of LTP fEPSP were recorded for 30 minutes. The fEPSP slopes were measured directly after the fiber volley to the peak or until the beginning of a clearly distinguishable population spike.

Analysis of LTP by whole cell patch clamp recording in CA1 pyramidal neurons

Whole-cell patch clamp recordings of CA1 pyramidal cells were performed in aCSF 2 with 100 µM picrotoxin. Glass pipettes were filled with internal solution (in mM): 115 potassium gluconate, 20 KCl, 10 HEPES, 4 Mg-ATP, 0.3. Na-GTP, 10 Na-phosphocreatine, 0.001 $CaCl_2$, (pH 7.4, 280-290 mosmol/l). SC were stimulated using glass pipette filled with aCSF2, at a frequency of 0.05 Hz and a stimulus duration of 70 µs. Input-output curve was measured for every cell and stimulation strength was adjusted to evoke an EPSP of 30-50% of the maximum EPSP. After a baseline recording of 10 min spike timing-dependent plasticity was induced by pairing a presynaptically evoked EPSP with 4 action potentials induced by postsynaptic current injection (3 ms lenght, 1 nA, 200 Hz) according to previously published protocols (Edelmann et al., 2015). This paring was repeated 35 times at 0.5Hz. Afterwards

EPSP were recorded for further 30 min. EPSP slopes were calculated from the initial 2 ms after EPSP onset. For analysis, the data were normalized to the average of the baseline recording (Edelmann et al., 2015).

Data acquisition and data analysis of electrophysiological recordings:

All Data were obtained using an EPC10 amplifier controlled by Patchmaster software (HEKA, Germany). mEPSC were analyzed using Clampfit 10 (Molecular Devices, USA). All other data were analyzed using NeuroMatic plugin (http://www.neuromatic.thinkrandom.com) of Igor Pro Software (Wavemetrics, Portland, OR, USA).

Generation of *Arc* expressing and negative control pAAV constructs

To generate a pAAV construct that codes for the murine *Arc* mRNA (indicated as ARC-AVV), the *Arc* cDNA open reading frame (ORF) was cut from a pCMV6-Entry_*Arc* vector (Origene, MR206218) by restriction digest using EcoRI and XhoI (Fermentas) and inserted into a p-AAV-Syn-iCre-2A-Venus vector (Tang et al., 2009) at the respective restriction sites using T4 Ligase (Fermentas). As negative control adaptor oligonucleotides have been generated by annealing two complementary noncoding sequences with EcoRI and XhoI restriction site overhangs (Neg(+): AATTgcatttgtactgacatct; Neg(-): TCGAagatgtcagtacaaatgc). This adaptor was ligated with the p-AAV-Syn-iCre-2A-Venus vector and linearized by EcoRI and XhoI treatment (indicated as CTRL AVV). Sequences of constructs were verified by Sanger sequencing at Eurofins Genomics, Ebersberg, Germany.

Virus production, isolation and quantification

48 hours prior to transfection, AAV-293 cells (Cell Biolabs Inc) were seeded at a density of 2x10^5 cells/cm2. When cells reached 70-80% confluency they were transfected using a reaction mix containing pRV1 (AAV2) (37.5 µg), pH21 (AAV1) (37.5 µg), pFdelta6 (Ad Helper) (150 µg), one of the pAAV constructs described above (75 µg), pEGFP-N3 (25 µg),

$CaCl_2$ (150 mM) and 1xHEPES buffered saline (HBS). The medium was replaced after 6h. 72 hours after transfection, cells were scraped in cold PBS and collected in reaction tubes. Cells were centrifuged at 800 x g for 10 minutes, cell pellets were resuspended and incubated for 1h at 37°C in a buffer containing 20 mM Tris, 159 mM NaCl (pH 8.0), 0.5% sodium deoxycholate and 50U/ml Benzonase. After two centrifugation steps at 3000 x g to remove cell debris, the AAV was isolated from the supernatant using heparin columns (GE Healthcare). After loading the column with the virus particles and washing with buffers containing 20 mM Tris and increasing concentrations of NaCl (100 mM, 200 mM, 300 mM), the virus was eluted using buffers containing 20 mM Tris and 400 mM, 450 mM and 500 mM NaCl. Virus was then concentrated using Amicon Ultra-4 centrifugal filter units (Merck-Millipore) and the solution was filtered with a 0.2 µm Acrodisc syringe filter (Sigma-Aldrich).

For virus quantification, the viral titer was determined using quantitative real-time PCR (qPCR). As a standard, the AAV plasmid construct was used to generate a dilution series with known concentrations. The diluted plasmid and the solutions containing AAV in an unknown concentration have been used as template for a PCR amplifying the Woodchuck Hepatitis Virus Posttranscriptional Regulatory Element (WPRE) using the oligonucleotides WPRE-F 5'-TGCTTCCCGTATGGCTTTCAT-3' and WPRE-R 5'-CAGCAAACACAGTGCACACC-3' as primers and SYBR Select Master Mix (ThermoFisher Scientific). The measurements were performed with a CFX384 instrument and analyses were done using the CFX Manager software (Biorad).

Immunohistochemistry

Animals were transcardially perfused with PBS and subsequently with 4% PFA under deep isoflurane anesthesia. The brains were post-fixed in 4% PFA for 24h at 4°C, cryoprotected in 10% and 30% sucrose in PBS and stored at -80°C. Coronal 40 µm slices were prepared on a sledge microtome equipped with a freezing unit (Thermo Fisher Scientific, Kalamazoo, USA). Slices were incubated in blocking buffer (TBS, 0,1% Triton X, 3% Serum, 2% skimed milk

powder) for 30 min. First antibody was incubated in blocking buffer over night at 4°C (anti-ARC/Arg3.1, Synaptic System, Göttingen, Germany, 1:500). Slices were washed in TBS and incubated with 2nd antibody for 2h at room temperature (Rhodamin@ guinea pig, Jackson ImmunoResearch, 1:300). Slices were mounted on gelatin-coated glass slides, stained with DAPI and embedded using Mowiol.

Golgi staining and dendritic spine analysis of CA1 pyramidal neurons

Morphological spine analysis was performed in pyramidal neurons of the CA1 region as described previously (Haselmann et al., 2018). Directly after removal of the mouse brain, brains were cut into hemispheres and one hemisphere was used for Golgi staining. Golgi silver impregnation was conducted with the FD Rapid GolgiStainTM Kit (FD NeuroTechnologies, Inc., Columbia, USA) according to manufacturer's instructions. Briefly, the tissue was rinsed in ACSF to remove blood residues, and was then transferred into equal amounts of solution A+B of the FD Rapid GolgiStainTM Kit. After renewal of solutions on the second day the tissue was subsequently left in the dark for 2 weeks at room temperature. Thereafter, brain hemispheres were transferred into solution C of the FD Rapid GolgiStainTM Kit, which was changed after one day, and were left in solution at C for 5 days. Hemispheres were then stored at 80°C until further use. Then, hemispheres were cut into 150mm thick coronal slices in the area of the hippocampus using a Leica CM3050S cryostat and mounted on object slides. For the last step of staining procedure, slices were washed in purified water (2x4 min), incubated in a mix of 1/4 solution D, 1/4 solution E and 1/2 purified water for 10 minutes, washed again, and then dehydrated in an ascending alcohol series (50%, 75%, 95% for 4 min each, and 100% for 8 min). Finally, slices were immersed in xylene (2x5 min), and then quickly coverslipped with Entellan® (Merck KGaG,Darmstadt, Germany) and dehumidified overnight. To evaluate dendritic morphology, a Zeiss Axioskop 2 mot plus and a computer-based system (Neurolucida; MicroBrightField) was used to generate three-dimensional neuron tracings that were subsequently analyzed using the NeuroExplorer

Software (MicroBrightField). Golgi-impregnated cells were selected for reconstruction if they fulfilled the following criteria: (1) the neuron was located within the pyramidal cell layer of the CA1 region (2) the neuron was distinguishable from neighboring cells to allow for identification of dendrites, (3) the dendrites were not truncated or broken, and (4) the cell exhibited dark and well filled impregnation throughout whole dendrites including spines. For analysis of dendritic spines, positively stained neurons in the CA region were randomly selected. Neuronal apical dendrites were followed up to tertiary branches without visible disruptions and without further split up using a Zeiss Axioskop 2 mot plus with an 100x oil immersion objective (PLAN-Neofluar, Zeiss). 3rd order branches of 20-50 µm stretch, 50-150 µm away from the soma of putative CA1 pyramidal cells were analyzed using Neurolicida Neuron Tracing Software. Spines were classified as follows: 1. Thin: shorter than 1,5 without swellings, 2: Mushroom: spine head larger than 0,6 µm 3. Stubby: length/width smaller than 1. Number and type of spines (mushroom, stubby, thin) were counted manually by the same blinded investigator. Total spine density was calculated as number of spines per 10 mm of dendritic length.

Analysis of Gene-expression and regulatory networks

Probe sampling

Isofluran anesthetized mice were sacrificed by decapitation and brains were harvested. Brain hemispheres were snap frozen in liquid nitrogen and brain tissue was stored at -80°C until further use.

RNA Isolation

Total RNA extraction was carried out using QIAzol lysis reagent and RNeasy Mini Kit (Qiagen, Hilden, Germany) according to manufacturer instructions; quality control of isolated RNA was performed on a QIAxcel capillary electrophoresis system (Qiagen, Hilden, Germany). Integrity of RNA was proven by reporting the 28S/18S ratio and the RIS number

(RNA Integrity Score) for analyzed samples. Quantification of total RNA and measuring the A260/A280 ratio was performed on a Nano-Drop spectrophotometer ND-2000 (Thermo Fisher Scientific, Schwerte, Germany).

Microarray Analysis

250 ng of total RNA of each sample was reversely transcribed and amplified using the TargetAmp-Nano Labeling Kit for Illumina Expression BeadChips (Biozym Scientific GmbH, Hessisch Oldendorf, Germany) on a Biorad MJ Thermal Cycler (Biorad, Munich, Germany) according to the manufacturer's instructions. All cRNA samples were purified with the NucleoSpin RNA Clean-up system (Macherey-Nagel, GmbH & Co. KG, Düren, Germany) and quantified on a Nano-Drop spectrophotometer ND-2000 (Thermo Fisher Scientific, Schwerte, Germany) before hybridization. Samples (750 ng cRNA) were hybridized 20 h, 58 °C on two Illumina MouseRef-8 v2.0 Expression BeadChips (Illumina, San Diego, CA, USA). Posthybridization data read-out, data preprocessing including spot detection, control probe quality check, background subtraction, signal averaging, and data analysis were performed with the Illumina GenomeStudio-Software v.2011.1 (Illumina, San Diego, CA, USA).

Data processing, gene set enrichment analysis and analysis of regulatory networks

Microarray data were preprocessed in the R statistical environment using the lumi package (Du et al., 2008), using log2-transformation and robust spline normalization (rsn). One sample ("9298740075_G") was identified as an outlier based on hierarchical clustering and was removed (Fig. S1A and B). Differentially expressed genes between PCI and Sham were determined using FDR/Benjamini-Hochberg correction and log2FC ≥ 1 cut-off. Gene set enrichment analysis for enriched Gene Ontology (GO) terms (category biological pathway) was performed using the piano package (Varemo et al., 2013). The raw and preprocessed data have been deposited in NCBI GEO DataSets with the following accession number: GSE167610.

Microarray data was further processed using the R environment (R Studio Version 1.1.383, R Version 3.6.1; RStudio Team, RStudio, Inc., Boston, MA, R Core Team, Foundation for Statistical Computing, Vienna, Austria) with the packages reshape2 (Wickham, 2007) and ggplot2. Networks were built and analyzed with the aid of Cytoscape (Version 3.8.0) including the apps Legend Creator (version 1.1.5) and stringApp (version 1.6.0) (Doncheva et al., 2019). Protein interactions were imported by the stringApp from the string data base for the species Mus musculus with a confidence cut-off ≥0.4.

Western Blot

Brains were snap frozen in liquid nitrogen and stored at -80°C until further use. Lysates were obtained using ice-cold RIPA buffer supplemented with complete protease inhibitor Kit and PhosSTOP inhibitor cocktail (both: Roche Diagnostics, Mannheim, Germany). The protein concentration was determined by Bradford Assay (BioRad Quick Start Bradford 1x Dye Reagent, #5000205). Proteins samples (30µg per lane) were subjected to SDS-Page and transferred to a PVDF membrane (Amersham™ Hybond®, GE Healthcare Life Science, United Kingdom). First antibodies were incubated overnight at 4°C (ARC/ARG3.1, 1:7500, #156005; Synaptic Systems GmbH, Germany; GAPDH, 1:10000, #2118L, Cell Signaling Technology, USA). Horse-radish peroxidase-labelled secondary antibodies (1:1000, Dianova, Germany) were incubated for 2h at room temperature. Chemiluminescent signals (Pierce ECL Western Bloting Substrate, Thermo Scientific, USA) were visualized using a luminescent image analyzer (LAS 3000, Fujifilm Life Science). Densitometric analysis was performed using ImageJ software. Regarding ARC expression 10 weeks after the PCI the summed signal of the ARC double band was used for analysis.

Capillary western immunoassay

Mouse hippocampi were homogenized in lysis buffer (0.32 M Sucrose, 4 mM Tris-HCL (pH = 7.4), 1 mM EDTA, 0.25 mM DTT) with additional ultrasound sonication (5x pulses). The

protein concentration was determined using Bradford assay (BioRad Quick Start Bradford 1x Dye Reagent, #5000205) prior to protein analysis by capillary western immunoassay (Wes™, ProteinSimple) according to the user manual. For each target, the antibody dilution and dynamic range has been determined independently to assure quantitative measurements. Proteins (0.2µg/µl) were separated in the 12-230 kD detection module (ProteinSimple, # SM-W004) and detected in multiplex assays with a-Tubulin (Cell Signaling Technology, #2144S, 1:10), Erk (Cell Signaling Technology, #4696, 1:10), and pErk (CellSignaling, #4370, 1:15) antibodies, respectively. The antibody incubation time of primary as well as of secondary antibodies was 30 min. The data from two separate experimental cohorts were normalized to the respective averaged SHAM levels. The normalized data were used for statistical analysis.

Data availability

The raw and preprocessed Microarray data have been deposited in NCBI GEO DataSets with the accession number GSE167610.

Statistical analysis

Data presented represent the median or the mean ± SEM as indicated in the figure legends. An unpaired, 2-sided Student's t test or a 2-way ANOVA (> 2 groups) was used to evaluate statistical significance using P less than 0.05 as the cutoff.

Acknowledgments

We thank C. Sommer, C. Reißig and D. Himsel for providing expert technical assistance. This work was supported by the Center of Sepsis Control and Care Jena (to CG, JW, HR, H-YC), the Schilling foundation (to CG), and intramural funding of Jena University Hospital (IZKF, to JW, HH, and H-YC).

Author contributions

CG and BG conceived and designed the experiments. BG, HH, HR, NHE, LG, MB and LS conducted in vitro experiments. BG, JW, HR, RAC performed the *in-vivo* experiments. BG, NHA, FH, H-YC, ASS, HR, AU, and RK analyzed the data. BG and NHA prepared the figures and CG wrote the manuscript. All authors have read and approved the final manuscript.

Disclosures: The authors declare no competing interests exist

References

Bischofberger, J., D. Engel, L. Li, J.R. Geiger, and P. Jonas. 2006. Patch-clamp recording from mossy fiber terminals in hippocampal slices. *Nat Protoc* 1:2075-2081. doi:10.1038/nprot.2006.312

Chung, H.Y., J. Wickel, F.M. Brunkhorst, and C. Geis. 2020. Sepsis-Associated Encephalopathy: From Delirium to Dementia? *J Clin Med* 9:doi:10.3390/jcm9030703

DaSilva, L.L.P., M.J. Wall, L. P. de Almeida, S.C. Wauters, Y.C. Januário, J. Müller, and S.A.L. Corrêa. 2016. Activity-Regulated Cytoskeleton-Associated Protein Controls AMPAR Endocytosis through a Direct Interaction with Clathrin-Adaptor Protein 2. *eneuro* 3:ENEURO.0144-0115.2016. doi:10.1523/eneuro.0144-15.2016

Doncheva, N.T., J.H. Morris, J. Gorodkin, and L.J. Jensen. 2019. Cytoscape StringApp: Network Analysis and Visualization of Proteomics Data. *J Proteome Res* 18:623-632. doi:10.1021/acs.jproteome.8b00702

Du, P., W.A. Kibbe, and S.M. Lin. 2008. lumi: a pipeline for processing Illumina microarray. *Bioinformatics* 24:1547-1548. doi:10.1093/bioinformatics/btn224

Edelmann, E., E. Cepeda-Prado, M. Franck, P. Lichtenecker, T. Brigadski, and V. Lessmann. 2015. Theta Burst Firing Recruits BDNF Release and Signaling in Postsynaptic CA1 Neurons in Spike-Timing-Dependent LTP. *Neuron* 86:1041-1054. doi:10.1016/j.neuron.2015.04.007

Eidelman, L.A., D. Putterman, C. Putterman, and C.L. Sprung. 1996. The spectrum of septic encephalopathy. Definitions, etiologies, and mortalities. *JAMA* 275:470-473.

Ely, E.W., A. Shintani, B. Truman, T. Speroff, S.M. Gordon, F.E. Harrell, Jr., S.K. Inouye, G.R. Bernard, and R.S. Dittus. 2004. Delirium as a predictor of mortality in mechanically ventilated patients in the intensive care unit. *JAMA* 291:1753-1762. doi:10.1001/jama.291.14.1753

Fleischmann, C., A. Scherag, N.K. Adhikari, C.S. Hartog, T. Tsaganos, P. Schlattmann, D.C. Angus, K. Reinhart, and T. International Forum of Acute Care. 2016. Assessment of Global Incidence and Mortality of Hospital-treated Sepsis. Current Estimates and Limitations. *Am J Respir Crit Care Med* 193:259-272. doi:10.1164/rccm.201504-0781OC

Gofton, T.E., and G.B. Young. 2012. Sepsis-associated encephalopathy. *Nat Rev Neurol* 8:557-566. doi:10.1038/nrneurol.2012.183

Gonnert, F.A., P. Recknagel, M. Seidel, N. Jbeily, K. Dahlke, C.L. Bockmeyer, J. Winning, W. Losche, R.A. Claus, and M. Bauer. 2011. Characteristics of clinical sepsis reflected in a reliable and reproducible rodent sepsis model. *J Surg Res* 170:e123-134. doi:10.1016/j.jss.2011.05.019

Grünewald, B., M.D. Lange, C. Werner, A. O'Leary, A. Weishaupt, S. Popp, D.A. Pearce, H. Wiendl, A. Reif, H.C. Pape, K.V. Toyka, C. Sommer, and C. Geis. 2017. Defective synaptic transmission causes disease signs in a mouse model of juvenile neuronal ceroid lipofuscinosis. *eLife* 6:e28685. doi:10.7554/eLife.28685

Guzowski, J.F., T. Miyashita, M.K. Chawla, J. Sanderson, L.I. Maes, F.P. Houston, P. Lipa, B.L. McNaughton, P.F. Worley, and C.A. Barnes. 2006. Recent behavioral history modifies coupling between cell activity and Arc gene transcription in hippocampal CA1 neurons. *Proc Natl Acad Sci U S A* 103:1077-1082. doi:10.1073/pnas.0505519103

Haselmann, H., F. Mannara, C. Werner, J. Planaguma, F. Miguez-Cabello, L. Schmidl, B. Grunewald, M. Petit-Pedrol, K. Kirmse, J. Classen, F. Demir, N. Klocker, D. Soto, S. Doose, J. Dalmau, S. Hallermann, and C. Geis. 2018. Human Autoantibodies against the AMPA Receptor Subunit GluA2 Induce Receptor Reorganization and Memory Dysfunction. *Neuron* 100:91-105 e109. doi:10.1016/j.neuron.2018.07.048

Haselmann, H., L. Ropke, C. Werner, A. Kunze, and C. Geis. 2015. Interactions of Human Autoantibodies with Hippocampal GABAergic Synaptic Transmission - Analyzing Antibody-Induced Effects ex vivo. *Front Neurol* 6:136. doi:10.3389/fneur.2015.00136

Huang, F., J.K. Chotiner, and O. Steward. 2007. Actin polymerization and ERK phosphorylation are required for Arc/Arg3.1 mRNA targeting to activated synaptic sites on dendrites. *J Neurosci* 27:9054-9067. doi:10.1523/JNEUROSCI.2410-07.2007

Jankowsky, J.L., T. Melnikova, D.J. Fadale, G.M. Xu, H.H. Slunt, V. Gonzales, L.H. Younkin, S.G. Younkin, D.R. Borchelt, and A.V. Savonenko. 2005. Environmental enrichment mitigates cognitive deficits in a mouse model of Alzheimer's disease. *J Neurosci* 25:5217-5224. doi:10.1523/JNEUROSCI.5080-04.2005

Jenks, K.R., T. Kim, E.D. Pastuzyn, H. Okuno, A.V. Taibi, H. Bito, M.F. Bear, and J.D. Shepherd. 2017. Arc restores juvenile plasticity in adult mouse visual cortex. *Proc Natl Acad Sci U S A* 114:9182-9187. doi:10.1073/pnas.1700866114

Kilkenny, C., W.J. Browne, I.C. Cuthill, M. Emerson, and D.G. Altman. 2010. Improving bioscience research reporting: the ARRIVE guidelines for reporting animal research. *PLoS Biol* 8:e1000412. doi:10.1371/journal.pbio.1000412

Korb, E., C.L. Wilkinson, R.N. Delgado, K.L. Lovero, and S. Finkbeiner. 2013. Arc in the nucleus regulates PML-dependent GluA1 transcription and homeostatic plasticity. *Nat Neurosci* 16:874-883. doi:10.1038/nn.3429

Li, L., J. Carter, X. Gao, J. Whitehead, and W.G. Tourtellotte. 2005. The neuroplasticity-associated arc gene is a direct transcriptional target of early growth response (Egr) transcription factors. *Mol Cell Biol* 25:10286-10300. doi:10.1128/MCB.25.23.10286-10300.2005

Mazeraud, A., C. Righy, E. Bouchereau, S. Benghanem, F.A. Bozza, and T. Sharshar. 2020. Septic-Associated Encephalopathy: a Comprehensive Review. *Neurotherapeutics* 17:392-403. doi:10.1007/s13311-020-00862-1

Michels, M., M. Abatti, A. Vieira, P. Avila, A.I. Goulart, H. Borges, E. Corneo, D. Dominguini, T. Barichello, and F. Dal-Pizzol. 2020. Modulation of microglial phenotypes improves sepsis-induced hippocampus-dependent cognitive impairments and decreases brain inflammation in an animal model of sepsis. *Clin Sci (Lond)* 134:765-776. doi:10.1042/CS20191322

Nagahara, A.H., D.A. Merrill, G. Coppola, S. Tsukada, B.E. Schroeder, G.M. Shaked, L. Wang, A. Blesch, A. Kim, J.M. Conner, E. Rockenstein, M.V. Chao, E.H. Koo, D. Geschwind, E. Masliah, A.A. Chiba, and M.H. Tuszynski. 2009. Neuroprotective effects of brain-derived neurotrophic factor in rodent and primate models of Alzheimer's disease. *Nat Med* 15:331-337. doi:10.1038/nm.1912

Okuno, H., K. Akashi, Y. Ishii, N. Yagishita-Kyo, K. Suzuki, M. Nonaka, T. Kawashima, H. Fujii, S. Takemoto-Kimura, M. Abe, R. Natsume, S. Chowdhury, K. Sakimura, P.F. Worley, and H. Bito. 2012. Inverse synaptic tagging of inactive synapses via dynamic interaction of Arc/Arg3.1 with CaMKIIbeta. *Cell* 149:886-898. doi:10.1016/j.cell.2012.02.062

Pak, J.H., F.L. Huang, J. Li, D. Balschun, K.G. Reymann, C. Chiang, H. Westphal, and K.P. Huang. 2000. Involvement of neurogranin in the modulation of calcium/calmodulin-dependent protein kinase II, synaptic plasticity, and spatial learning: a study with knockout mice. *Proc Natl Acad Sci U S A* 97:11232-11237. doi:10.1073/pnas.210184697

Pandharipande, P.P., T.D. Girard, J.C. Jackson, A. Morandi, J.L. Thompson, B.T. Pun, N.E. Brummel, C.G. Hughes, E.E. Vasilevskis, A.K. Shintani, K.G. Moons, S.K. Geevarghese, A. Canonico, R.O. Hopkins, G.R. Bernard, R.S. Dittus, E.W. Ely, and B.-I.S. Investigators. 2013. Long-term cognitive impairment after critical illness. *N Engl J Med* 369:1306-1316. doi:10.1056/NEJMoa1301372

Panja, D., and C.R. Bramham. 2014. BDNF mechanisms in late LTP formation: A synthesis and breakdown. *Neuropharmacology* 76 Pt C:664-676. doi:10.1016/j.neuropharm.2013.06.024

Peca, J., C. Feliciano, J.T. Ting, W. Wang, M.F. Wells, T.N. Venkatraman, C.D. Lascola, Z. Fu, and G. Feng. 2011. Shank3 mutant mice display autistic-like behaviours and striatal dysfunction. *Nature* 472:437-442. doi:10.1038/nature09965

Petit-Pedrol, M., J. Sell, J. Planaguma, F. Mannara, M. Radosevic, H. Haselmann, M. Ceanga, L. Sabater, M. Spatola, D. Soto, X. Gasull, J. Dalmau, and C. Geis. 2018. LGI1

antibodies alter Kv1.1 and AMPA receptors changing synaptic excitability, plasticity and memory. *Brain* 141:3144-3159. doi:10.1093/brain/awy253

Planaguma, J., H. Haselmann, F. Mannara, M. Petit-Pedrol, B. Grunewald, E. Aguilar, L. Ropke, E. Martin-Garcia, M.J. Titulaer, P. Jercog, F. Graus, R. Maldonado, C. Geis, and J. Dalmau. 2016. Ephrin-B2 prevents N-methyl-D-aspartate receptor antibody effects on memory and neuroplasticity. *Ann Neurol* 80:388-400. doi:10.1002/ana.24721

Plath, N., O. Ohana, B. Dammermann, M.L. Errington, D. Schmitz, C. Gross, X. Mao, A. Engelsberg, C. Mahlke, H. Welzl, U. Kobalz, A. Stawrakakis, E. Fernandez, R. Waltereit, A. Bick-Sander, E. Therstappen, S.F. Cooke, V. Blanquet, W. Wurst, B. Salmen, M.R. Bosl, H.P. Lipp, S.G. Grant, T.V. Bliss, D.P. Wolfer, and D. Kuhl. 2006. Arc/Arg3.1 is essential for the consolidation of synaptic plasticity and memories. *Neuron* 52:437-444. doi:10.1016/j.neuron.2006.08.024

Ramirez-Amaya, V., A. Vazdarjanova, D. Mikhael, S. Rosi, P.F. Worley, and C.A. Barnes. 2005. Spatial exploration-induced Arc mRNA and protein expression: evidence for selective, network-specific reactivation. *J Neurosci* 25:1761-1768. doi:10.1523/JNEUROSCI.4342-04.2005

Rial Verde, E.M., J. Lee-Osbourne, P.F. Worley, R. Malinow, and H.T. Cline. 2006. Increased expression of the immediate-early gene arc/arg3.1 reduces AMPA receptor-mediated synaptic transmission. *Neuron* 52:461-474. doi:10.1016/j.neuron.2006.09.031

Semmler, A., S. Hermann, F. Mormann, M. Weberpals, S.A. Paxian, T. Okulla, M. Schafers, M.P. Kummer, T. Klockgether, and M.T. Heneka. 2008. Sepsis causes neuroinflammation and concomitant decrease of cerebral metabolism. *J Neuroinflammation* 5:38. doi:10.1186/1742-2094-5-38

Shemer, A., I. Scheyltjens, G.R. Frumer, J.S. Kim, J. Grozovski, S. Ayanaw, B. Dassa, H. Van Hove, L. Chappell-Maor, S. Boura-Halfon, D. Leshkowitz, W. Mueller, N. Maggio, K. Movahedi, and S. Jung. 2020. Interleukin-10 Prevents Pathological Microglia Hyperactivation following Peripheral Endotoxin Challenge. *Immunity* 53:1033-1049 e1037. doi:10.1016/j.immuni.2020.09.018

Shepherd, J.D., and M.F. Bear. 2011. New views of Arc, a master regulator of synaptic plasticity. *Nat Neurosci* 14:279-284. doi:10.1038/nn.2708

Shepherd, J.D., G. Rumbaugh, J. Wu, S. Chowdhury, N. Plath, D. Kuhl, R.L. Huganir, and P.F. Worley. 2006. Arc/Arg3.1 mediates homeostatic synaptic scaling of AMPA receptors. *Neuron* 52:475-484. doi:10.1016/j.neuron.2006.08.034

Singer, M., C.S. Deutschman, C.W. Seymour, M. Shankar-Hari, D. Annane, M. Bauer, R. Bellomo, G.R. Bernard, J.D. Chiche, C.M. Coopersmith, R.S. Hotchkiss, M.M. Levy, J.C. Marshall, G.S. Martin, S.M. Opal, G.D. Rubenfeld, T. van der Poll, J.L. Vincent, and D.C. Angus. 2016. The Third International Consensus Definitions for Sepsis and Septic Shock (Sepsis-3). *JAMA* 315:801-810. doi:10.1001/jama.2016.0287

Tang, W., I. Ehrlich, S.B. Wolff, A.M. Michalski, S. Wolfl, M.T. Hasan, A. Luthi, and R. Sprengel. 2009. Faithful expression of multiple proteins via 2A-peptide self-processing: a versatile and reliable method for manipulating brain circuits. *J Neurosci* 29:8621-8629. doi:10.1523/JNEUROSCI.0359-09.2009

Taquet, M., S. Luciano, J.R. Geddes, and P.J. Harrison. 2021. Bidirectional associations between COVID-19 and psychiatric disorder: retrospective cohort studies of 62 354 COVID-19 cases in the USA. *Lancet Psychiatry* 8:130-140. doi:10.1016/S2215-0366(20)30462-4

Trzeciak, A., Y.V. Lerman, T.H. Kim, M.R. Kim, N. Mai, M.W. Halterman, and M. Kim. 2019. Long-Term Microgliosis Driven by Acute Systemic Inflammation. *J Immunol* 203:2979-2989. doi:10.4049/jimmunol.1900317

van Praag, H., G. Kempermann, and F.H. Gage. 2000. Neural consequences of environmental enrichment. *Nat Rev Neurosci* 1:191-198. doi:10.1038/35044558

Varemo, L., J. Nielsen, and I. Nookaew. 2013. Enriching the gene set analysis of genome-wide data by incorporating directionality of gene expression and combining statistical hypotheses and methods. *Nucleic Acids Res* 41:4378-4391. doi:10.1093/nar/gkt111

Vazdarjanova, A., V. Ramirez-Amaya, N. Insel, T.K. Plummer, S. Rosi, S. Chowdhury, D. Mikhael, P.F. Worley, J.F. Guzowski, and C.A. Barnes. 2006. Spatial exploration induces ARC, a plasticity-related immediate-early gene, only in calcium/calmodulin-dependent protein kinase II-positive principal excitatory and inhibitory neurons of the rat forebrain. *J Comp Neurol* 498:317-329. doi:10.1002/cne.21003

Wickham, H. 2007. Reshaping Data with the reshape Package. *2007* 21:20. doi:10.18637/jss.v021.i12

Widmann, C.N., and M.T. Heneka. 2014. Long-term cerebral consequences of sepsis. *The Lancet Neurology* 13:630-636. doi:10.1016/s1474-4422(14)70017-1

Yin, Y., G.M. Edelman, and P.W. Vanderklish. 2002. The brain-derived neurotrophic factor enhances synthesis of Arc in synaptoneurosomes. *Proc Natl Acad Sci U S A* 99:2368-2373. doi:10.1073/pnas.042693699

Zhang, W., J. Wu, M.D. Ward, S. Yang, Y.A. Chuang, M. Xiao, R. Li, D.J. Leahy, and P.F. Worley. 2015. Structural basis of arc binding to synaptic proteins: implications for cognitive disease. *Neuron* 86:490-500. doi:10.1016/j.neuron.2015.03.030

Zhao, S., J.T. Ting, H.E. Atallah, L. Qiu, J. Tan, B. Gloss, G.J. Augustine, K. Deisseroth, M. Luo, A.M. Graybiel, and G. Feng. 2011. Cell type-specific channelrhodopsin-2 transgenic mice for optogenetic dissection of neural circuitry function. *Nat Methods* 8:745-752. doi:10.1038/nmeth.1668

Zrzavy, T., R. Hoftberger, T. Berger, H. Rauschka, O. Butovsky, H. Weiner, and H. Lassmann. 2019. Pro-inflammatory activation of microglia in the brain of patients with sepsis. *Neuropathol Appl Neurobiol* 45:278-290. doi:10.1111/nan.12502

Figures and figure legends

Figure 1. Experimental sepsis causes neurocognitive dysfunction, defective long-term potentiation, and synaptic scaling in excitatory synapses. (A) Experimental schematic: acute phase of PCI is marked in red. Antibiotics (ATB) are delivered i.p. until day 10 and behavioral testing (open field, OF; elevated plus maze, EPM; Morris water maze, WMW) and *ex-vivo* electrophysiological recordings (long-term potentiation, LTP, and patch-clamp recordings, PC) are performed at the indicated time points. **(B)** Kaplan-Meier survival curve of experimental animals (left). Mice intentionally leaving the study e.g. for tissue harvesting were included up to the time when they are censored. Mean and distribution of sepsis severity score (CSS) on day 3 and on day 5 after PCI (right; each circle represents an individual mouse after PCI). **(C)** In the MWM PCI mice (n = 12, red) show affected learning (left; 2-way ANOVA) and reduced memory recall in the probe trial (right; example tracking traces are shown, target quadrant in dark grey; SHAM mice n = 18, blue). **(D)** PCI mice spent reduced time in the EPM open arms (light grey). The locomotor activity as measured by total distance traveled within the EPM is unchanged (n = 12/7; SHAM/PCI). **(E)** PCI mice spent reduced time the OF center (dark grey), whereas the distance traveled within the OF as a measure for locomotor activity is unchanged (n = 20/15; SHAM/PCI). **(F)** LTP in the hippocampal Schaffer collateral – CA1 pathway is severely impaired in PCI mice (n = 7; SHAM: n = 12; 2-way ANOVA). Inset shows average traces of example recordings before and after theta burst stimulation. **(G to I)** Patch-clamp recordings of dentate gyrus granule cells indicates reduced frequency of miniature (m) and spontaneous (s)EPSC, and increased peak amplitude of minimally evoked (eEPSC), mEPSC, and sEPSC (PCI: n = 11/13/13, SHAM: n = 11/13/16, respectively). Example traces in (G) and (H), average traces of minimal

evoked eEPSC in (I). Bar graphs show mean ± SEM; 2-tailed Student's t test, unless otherwise indicated. *P < 0.05; **P < 0.05.

Figure 2: PCI leads to distinct and time-dependent changes in gene expression. GO terms enriched in differently expressed genes (144 DEGs; $log_2FC > 1$) found by microarray analysis of brain tissue at 3 days and 10 weeks after PCI. Differentially expressed genes were interrogated for enrichment in the gene sets of the Gene Ontology definitions employing the piano package. Significantly enriched gene sets were clustered according to the score values of the five piano criteria distinct directional (up and down), mixed directional (up and down) and non-directional.

Figure 3. PCI induces downregulation of neuronal pathways mediating synaptic plasticity. (A) Interaction network of proteins corresponding to DEGs on day 3 after PCI. The node color depicts the respective Log_2FC from microarray data. Proteins related to ARC synaptic signaling are highlighted by size. **(B)** Expression of seven selected DEGs that are related to ARC signaling and synaptic function (highlighted in A). 3 days SHAM and PCI and 10 weeks PCI n = 4, 10 weeks SHAM n = 3. Boxplots show median and 75th to 25th interquartile range, whiskers show respective maximum or minimum values within 1.5 times of the interquartile range; 2-tailed Student's t test. **(C** and **D)** Quantitative analysis of hippocampal ARC protein and pErk/Erk protein ratio (n = 8, each; normalized to SHAM ARC or SHAM pERK/ERK ratio, respectively) shows downregulation of signaling pathways in the network shown in (A). 2-tailed Student's t test. *P < 0.05, **P < 0.01.

Figure 4. Hippocampal overexpression of ARC rescues sepsis-induced cognitive dysfunction and defective long-term potentiation. (A) Experimental schedule indicating ARC overexpression in the hippocampus from day 10 after PCI. Stereotactic

intrahippocampal microinjection of an adeno-associated virus (AAV) containing the bicistronic vector for ARC overexpression and Venus fluorescence under the synapsin promotor at the indicated coordinates. **(B)** Representative example of constitutive ARC overexpression in the CA3 region of the hippocampus. Scale bars: 40 µm. **(C)** PCI mice receiving control AAV (PCI CTRL AAV; n = 17) show learning deficits in the Barnes Maze compared to SHAM CTRL AAV (n = 18) as indicated by prolonged time to the target hole (upper panel) and reduced time in the target zone in the probe trail (day 7, lower panel). ARC overexpression in PCI mice (PCI ARC AAV; n = 18) results in rescue of learning and memory dysfunction. Example traces indicate tracks of individual mice during the probe trial; the target quadrant containing the open hole is marked in grey. **(D)** LTP as measured by slope of excitatory postsynaptic potentials (EPSP) in single-cell whole cell recordings in CA1 neurons after stimulation of Schaffer collaterals. Paired stimulation results in LTP in SHAM CTRL AAV (n = 11) and PCI ARC AAV (n = 8) mice whereas PCI mice with control virus injection (PCI CTRL AAV; n = 9) show reduced LTP. Left panel: average traces (blue: SHAM CTRL AAV; red: PCI CTRL AAV; light red: PCI ARC AAV). Middle panel: LTP time course. Right panel: comparison of LTP at the indicated time points after theta burst stimulation. 2-way ANOVA with Tukey's post hoc test. *P < 0.05, **P < 0.01.

Figure 5. Enriched environment leads to improvement of synaptic pathology and cognitive dysfunction after PCI. (A) Mice were subjected to enriched environment (EE) or standard housing (NE) from day 10 after PCI. **(B)** EE improves cognitive dysfunction in the BM after PCI (PCI EE) as indicated by reduced time to target hole in the training phase (left) and by increased time in the BM target zone during the probe trial compared to PCI mice in standard care (PCI NE). Example traces indicate tracks of individual mice during the probe trial; target quadrant is marked in grey. **(C)** EE leads to reduced anxiety-related behavior in the EPM after PCI as shown by reduced time in the closed and increased time in the open arms; n = 14 / 18 / 13 / 16; SHAM NE / SHAM EE / PCI NE / PCI EE in B and C). **(D)** LTP as evaluated by field potential recording in CA1 is improved in PCI mice after EE. Left panel:

average traces before and after theta burst stimulation (SHAM EE light blue; PCI EE light red; amplitudes of the baseline traces of each group were scaled to the amplitude of the SHAM NE trace (dark blue). Right panel: comparison of LTP at the indicated time points after theta burst stimulation; bottom panel: LTP time course. **(E)** Quantification of synaptic mushroom spines in apical dendrites of CA1 neurons. Example images are provided (scale bar: 5 µm). PCI leads to reduction of mature mushroom spine density (PCI NE) which is rescued to basal levels (SHAM NE) after enriched environment (PCI EE); n = 42 / 21 / 33 / 36; SHAM NE / SHAM EE / PCI NE / PCI EE. 2-way ANOVA with Tukey`s post hoc test. *P < 0.05, **P < 0.01, ***P < 0.001.

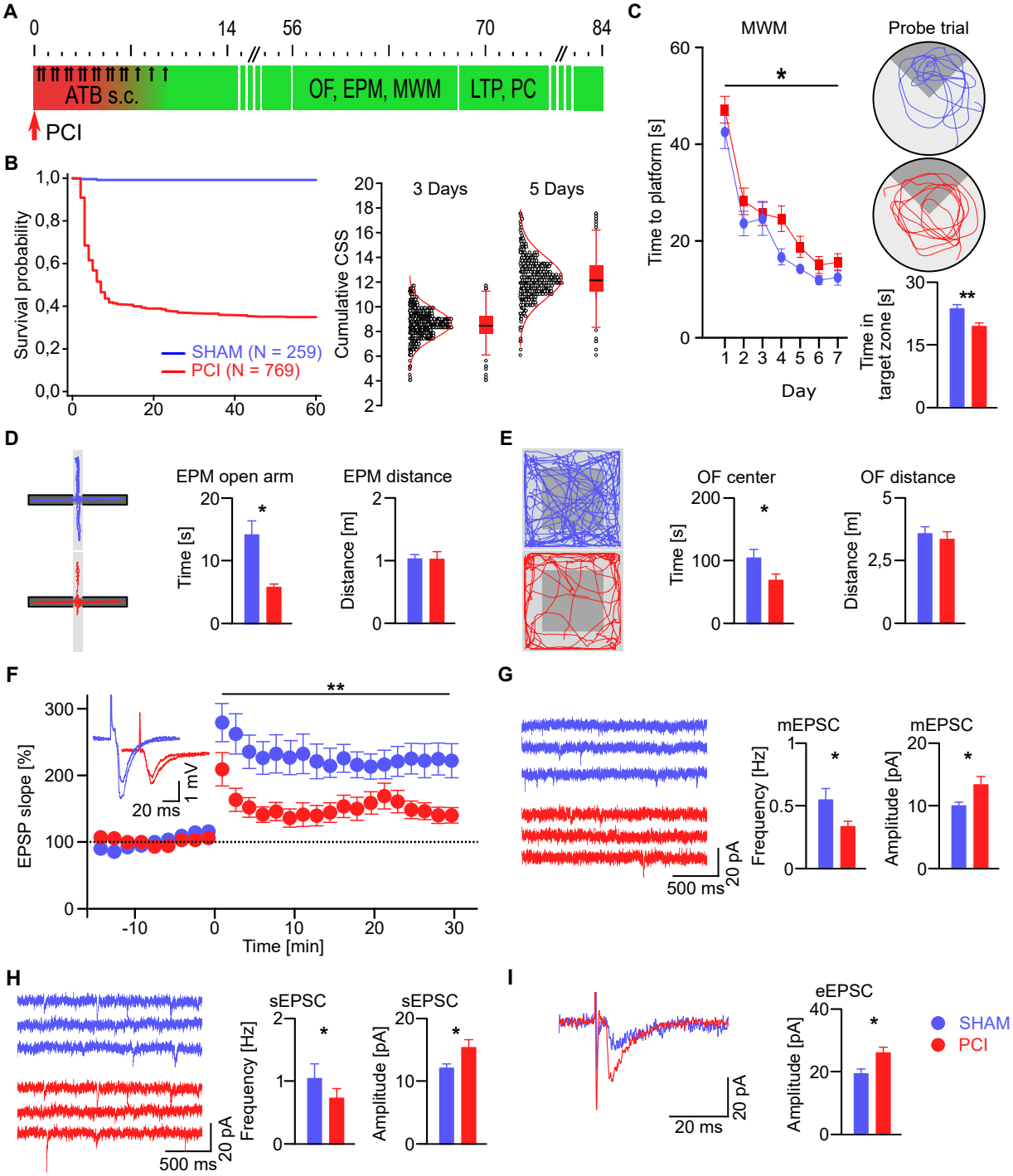
A
0
14
56
70
84
ATB s.c.
OF, EPM, MWM
LTP, PC
PCI
B
Survival probability
SHAM (N = 259)
PCI (N = 769)
Cumulative CSS
3 Days
5 Days
C
MWM
Probe trial
Time to platform [s]
Day
Time in target zone [s]
D
EPM open arm
EPM distance
Time [s]
Distance [m]
E
OF center
OF distance
Time [s]
Distance [m]
F
EPSP slope [%]
20 ms
1 mV
Time [min]
G
mEPSC
mEPSC
Frequency [Hz]
Amplitude [pA]
500 ms
20 pA
H
sEPSC
sEPSC
Frequency [Hz]
Amplitude [pA]
500 ms
20 pA
I
eEPSC
Amplitude [pA]
20 ms
20 pA
SHAM
PCI

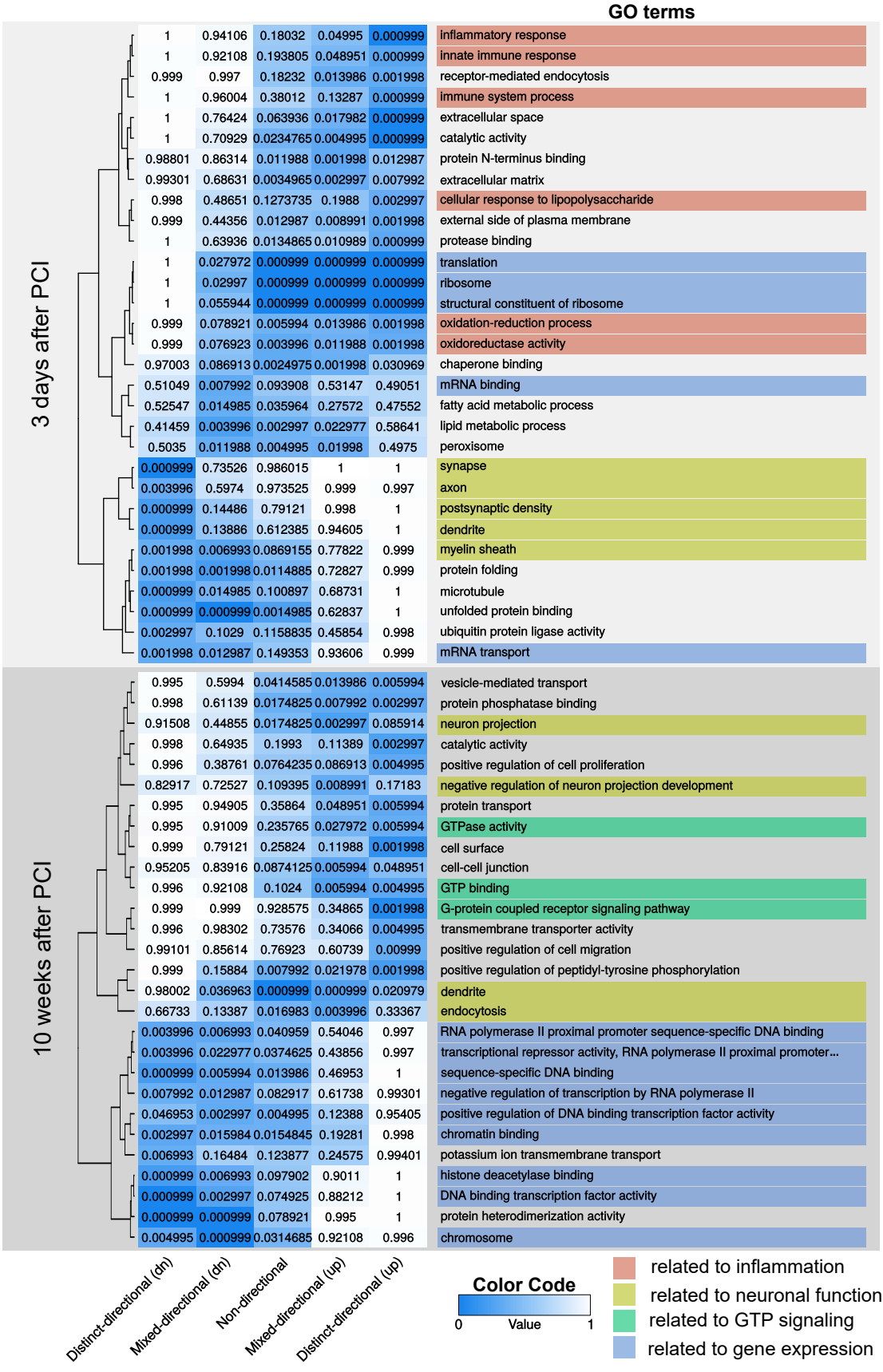

GO terms	Distinct-directional (dn)	Mixed-directional (dn)	Non-directional	Mixed-directional (up)	Distinct-directional (up)
inflammatory response	1	0.94106	0.18032	0.04995	0.000999
innate immune response	1	0.92108	0.193805	0.048951	0.000999
receptor-mediated endocytosis	0.999	0.997	0.18232	0.013986	0.001998
immune system process	1	0.96004	0.38012	0.13287	0.000999
extracellular space	1	0.76424	0.063936	0.017982	0.000999
catalytic activity	1	0.70929	0.0234765	0.004995	0.000999
protein N-terminus binding	0.98801	0.86314	0.011988	0.001998	0.012987
extracellular matrix	0.99301	0.68631	0.0034965	0.002997	0.007992
cellular response to lipopolysaccharide	0.998	0.48651	0.1273735	0.1988	0.002997
external side of plasma membrane	0.999	0.44356	0.012987	0.008991	0.001998
protease binding	1	0.63936	0.0134865	0.010989	0.000999
translation	1	0.027972	0.000999	0.000999	0.000999
ribosome	1	0.02997	0.000999	0.000999	0.000999
structural constituent of ribosome	1	0.055944	0.000999	0.000999	0.000999
oxidation-reduction process	0.999	0.078921	0.005994	0.013986	0.001998
oxidoreductase activity	0.999	0.076923	0.003996	0.011988	0.001998
chaperone binding	0.97003	0.086913	0.0024975	0.001998	0.030969
mRNA binding	0.51049	0.007992	0.093908	0.53147	0.49051
fatty acid metabolic process	0.52547	0.014985	0.035964	0.27572	0.47552
lipid metabolic process	0.41459	0.003996	0.002997	0.022977	0.58641
peroxisome	0.5035	0.011988	0.004995	0.01998	0.4975
synapse	0.000999	0.73526	0.986015	1	1
axon	0.003996	0.5974	0.973525	0.999	0.997
postsynaptic density	0.000999	0.14486	0.79121	0.998	1
dendrite	0.000999	0.13886	0.612385	0.94605	1
myelin sheath	0.001998	0.006993	0.0869155	0.77822	0.999
protein folding	0.001998	0.001998	0.0114885	0.72827	0.999
microtubule	0.000999	0.014985	0.100897	0.68731	1
unfolded protein binding	0.000999	0.000999	0.0014985	0.62837	1
ubiquitin protein ligase activity	0.002997	0.1029	0.1158835	0.45854	0.998
mRNA transport	0.001998	0.012987	0.149353	0.93606	0.999
vesicle-mediated transport	0.995	0.5994	0.0414585	0.013986	0.005994
protein phosphatase binding	0.998	0.61139	0.0174825	0.007992	0.002997
neuron projection	0.91508	0.44855	0.0174825	0.002997	0.085914
catalytic activity	0.998	0.64935	0.1993	0.11389	0.002997
positive regulation of cell proliferation	0.996	0.38761	0.0764235	0.086913	0.004995
negative regulation of neuron projection development	0.82917	0.72527	0.109395	0.008991	0.17183
protein transport	0.995	0.94905	0.35864	0.048951	0.005994
GTPase activity	0.995	0.91009	0.235765	0.027972	0.005994
cell surface	0.999	0.79121	0.25824	0.11988	0.001998
cell-cell junction	0.95205	0.83916	0.0874125	0.005994	0.048951
GTP binding	0.996	0.92108	0.1024	0.005994	0.004995
G-protein coupled receptor signaling pathway	0.999	0.999	0.928575	0.34865	0.001998
transmembrane transporter activity	0.996	0.98302	0.73576	0.34066	0.004995
positive regulation of cell migration	0.99101	0.85614	0.76923	0.60739	0.00999
positive regulation of peptidyl-tyrosine phosphorylation	0.999	0.15884	0.007992	0.021978	0.001998
dendrite	0.98002	0.036963	0.000999	0.000999	0.020979
endocytosis	0.66733	0.13387	0.016983	0.003996	0.33367
RNA polymerase II proximal promoter sequence-specific DNA binding	0.003996	0.006993	0.040959	0.54046	0.997
transcriptional repressor activity, RNA polymerase II proximal promoter...	0.003996	0.022977	0.0374625	0.43856	0.997
sequence-specific DNA binding	0.000999	0.005994	0.013986	0.46953	1
negative regulation of transcription by RNA polymerase II	0.007992	0.012987	0.082917	0.61738	0.99301
positive regulation of DNA binding transcription factor activity	0.046953	0.002997	0.004995	0.12388	0.95405
chromatin binding	0.002997	0.015984	0.0154845	0.19281	0.998
potassium ion transmembrane transport	0.006993	0.16484	0.123877	0.24575	0.99401
histone deacetylase binding	0.000999	0.006993	0.097902	0.9011	1
DNA binding transcription factor activity	0.000999	0.002997	0.074925	0.88212	1
protein heterodimerization activity	0.000999	0.000999	0.078921	0.995	1
chromosome	0.004995	0.000999	0.0314685	0.92108	0.996

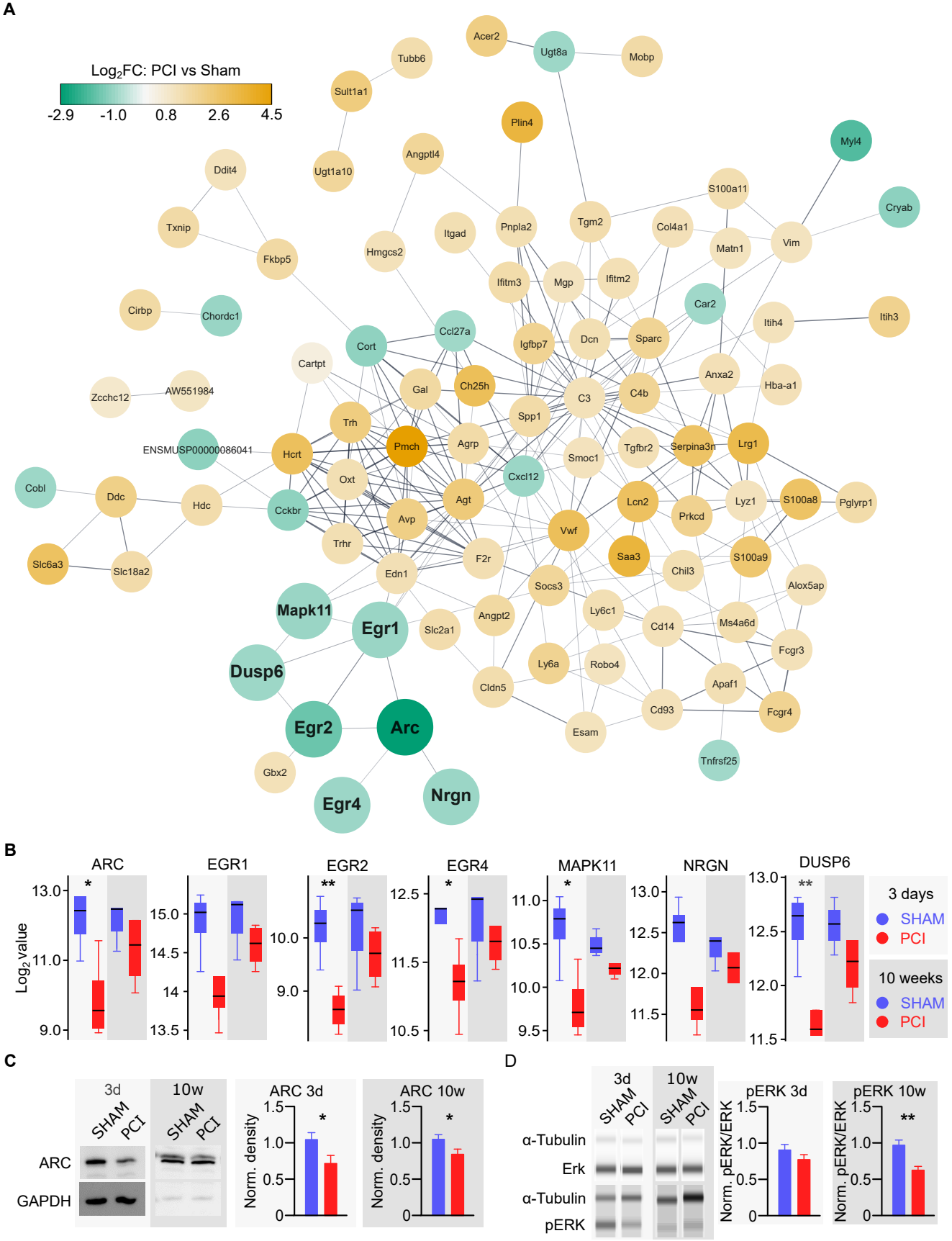
A
Log2FC: PCI vs Sham
-2.9
-1.0
0.8
2.6
4.5
Acer2
Ugt8a
Mobp
Tubb6
Sult1a1
Plin4
Myl4
Ugt1a10
Angptl4
Ddit4
S100a11
Cryab
Txnip
Itgad
Pnpla2
Tgm2
Col4a1
Vim
Fkbp5
Hmgcs2
Matn1
Ifitm3
Mgp
Ifitm2
Car2
Cirbp
Chordc1
Itih4
Itih3
Ccl27a
Cort
Igfbp7
Dcn
Sparc
Cartpt
Anxa2
Hba-a1
Zcchc12
AW551984
Gal
Ch25h
C3
C4b
Trh
Spp1
ENSMUSP00000086041
Hcrt
Pmch
Agrp
Smoc1
Tgfbr2
Serpina3n
Lrg1
Cobl
Ddc
Oxt
Cxcl12
Hdc
Cckbr
Agt
Lcn2
Lyz1
S100a8
Pglyrp1
Avp
Prkcd
Vwf
Trhr
Saa3
S100a9
Slc6a3
Slc18a2
F2r
Chil3
Edn1
Socs3
Alox5ap
Mapk11
Egr1
Angpt2
Ly6c1
Cd14
Ms4a6d
Slc2a1
Fcgr3
Dusp6
Ly6a
Robo4
Cldn5
Apaf1
Cd93
Fcgr4
Egr2
Arc
Esam
Tnfrsf25
Gbx2
Egr4
Nrgn
B
ARC
EGR1
EGR2
EGR4
MAPK11
NRGN
DUSP6
Log2 value
3 days
SHAM
PCI
10 weeks
SHAM
PCI
C
3d
10w
SHAM
PCI
SHAM
PCI
ARC
GAPDH
ARC 3d
ARC 10w
Norm. density
D
3d
10w
SHAM
PCI
SHAM
PCI
α-Tubulin
Erk
α-Tubulin
pERK
pERK 3d
pERK 10w
Norm. pERK/ERK

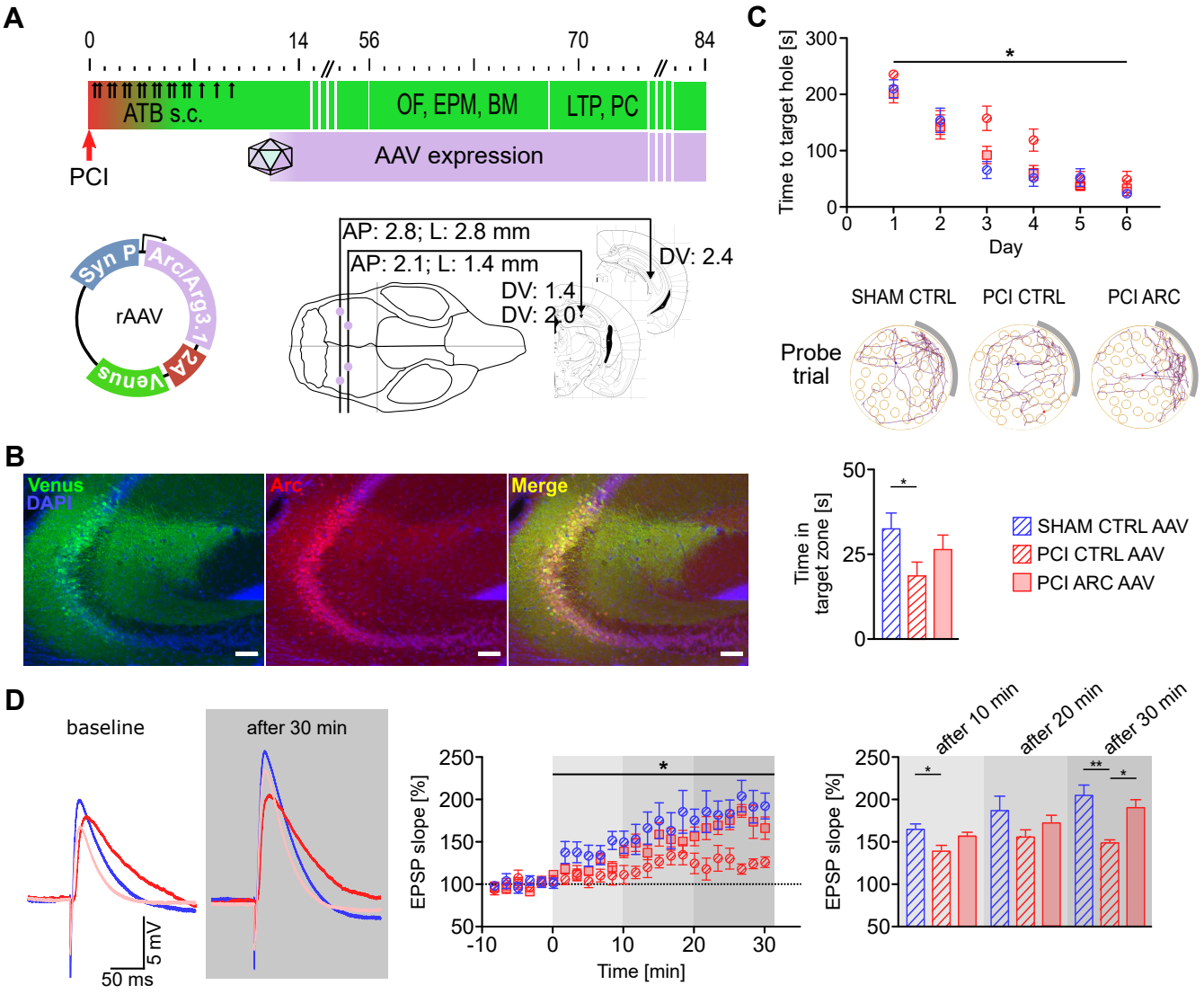
A
0
14
56
70
84
ATB s.c.
OF, EPM, BM
LTP, PC
PCI
AAV expression
Syn P
Arc/Arg3.1
2A
Venus
rAAV
AP: 2.8; L: 2.8 mm
AP: 2.1; L: 1.4 mm
DV: 1.4
DV: 2.0
DV: 2.4
C
Time to target hole [s]
Day
SHAM CTRL
PCI CTRL
PCI ARC
Probe trial
B
Venus
DAPI
Arc
Merge
Time in target zone [s]
SHAM CTRL AAV
PCI CTRL AAV
PCI ARC AAV
D
baseline
after 30 min
5 mV
50 ms
EPSP slope [%]
Time [min]
after 10 min
after 20 min
after 30 min

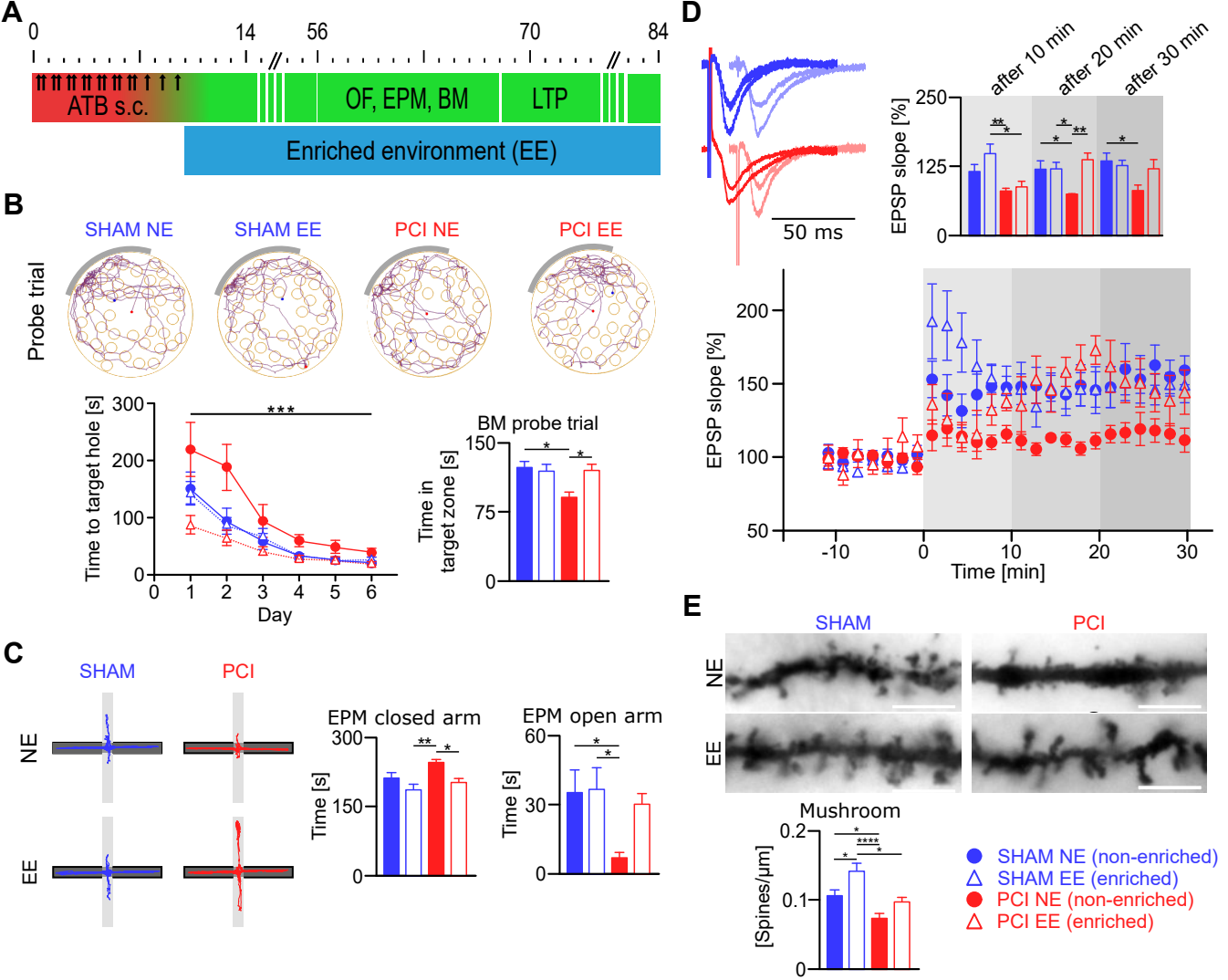
A
0
14
56
70
84
ATB s.c.
OF, EPM, BM
LTP
Enriched environment (EE)
B
SHAM NE
SHAM EE
PCI NE
PCI EE
Probe trial
Time to target hole [s]
Day
***
BM probe trial
Time in target zone [s]
C
SHAM
PCI
NE
EE
EPM closed arm
EPM open arm
Time [s]
D
50 ms
after 10 min
after 20 min
after 30 min
EPSP slope [%]
Time [min]
E
SHAM
PCI
NE
EE
Mushroom
[Spines/µm]
SHAM NE (non-enriched)
SHAM EE (enriched)
PCI NE (non-enriched)
PCI EE (enriched)